Computational simulations of MR elastography in idealised abdominal aortic aneurysms

Computational Simulations of MR Elastography in Idealised Abdominal Aortic Aneurysms

L Hollis[1], N Conlisk[1], L E J Thomas-Seale[1], N Roberts[2], P Pankaj[3] and P R Hoskins[1]

[1] University of Edinburgh, Centre for Cardiovascular Sciences, 47 Little France Crescent, Edinburgh, EH16 4TJ, UK

[2] University of Edinburgh, Clinical Research Imaging Centre, 47 Little France Crescent, Edinburgh, EH16 4TJ, UK

[3] University of Edinburgh, School of Engineering, The King's Buildings, EH9 3JL, UK

E-mail: lyamhollis@outlook.com

April 2016

Abstract.

Introduction Patient specific modelling (PSM) of abdominal aortic aneurysm (AAA) aims to predict rupture risk by calculating the peak stress acting on the AAA wall using finite element analysis (FEA). It is hypothesised that magnetic resonance elastography (MRE), a non-invasive technique measuring material properties, can improve PSM by allowing integration of patient specific properties into the model. MRE measurements are, however, dependent on the geometry under investigation as well as the material properties. This preliminary study used FEA to investigate the ability of MRE to achieve reproducible measurements of the elastic properties of the thrombus in different sized idealised AAA geometries.

Methods Idealised AAA geometries of diameter 50, 60 and 70 mm were created with material properties based on literature values prescribed. FEA was run with frequencies of 50, 100, and 120 Hz induced into the model. Synthetic noise was applied to the models and the ability of a 3-D Butterworth bandpass filter to remove it's influence was assessed.

Results and Discussion In low prescribed shear moduli greatest accuracy was typically achieved at 50 Hz, contrasting with high prescribed shear moduli, where it was achieved at 120 Hz. Variation in measurements across the three AAAs was lowest at 120 Hz with a mean coefficient of variation across all prescribed shear moduli of 9% in contrast to 11 and 18% at 100 and 50 Hz respectively. Bandpass filtering was able to fully recover material property measurements at noise levels of 1 and 2%, but was unable to do so for high prescribed shear modulus values at levels above this.

Conclusions Of the frequencies tested here, 120 Hz achieved the most reproducible measurements across the three AAA sizes, though accuracy of measurements at this frequency was compromised in low prescribed shear moduli.

Keywords: magnetic resonance elastography, finite element analysis, abdominal aortic aneurysm, patient specific modelling.

1. Introduction

Patient specific modelling (PSM) utilises individual patient data to construct computational models of human pathophysiology in order to improve the diagnosis and prognosis prediction of diseases [1, 2]. Typically finite element analysis (FEA) may be used for calculation of stresses within the tissues whilst computational fluid dynamic (CFD) is used for calculation of the blood flow field and wall shear stress of the blood on vessel walls [3, 4]. There are however several limitations to patient specific modelling [5, 6] particularly in relation to the application of material properties. In FEA the modelling process requires definition of the material properties of the tissues, such as density and elastic properties, however, it is not possible to obtain this information from either traditional MRI or CT. It is therefore common practice to use population average values of density and elastic properties obtained from mechanical testing of tissue samples. In FEA of stress in abdominal aortic aneurysm (AAA) the values of elastic properties typically used are those measured by Raghavan and Vorp (2000) [7] for the vessel wall and Wang et al. (2002) for the thrombus [8]. In this way, PSM has been used to estimate wall stress in abdominal aortic aneurysm in an attempt to provide improved rupture prediction over conventional use of maximum diameter [9, 10, 11, 12, 13]. The availability of elastic properties of tissues which are specific to the individual patient is likely to lead to improved accuracy of stress estimation, and longer term this should lead to improved ability to predict key events such as aneurysm rupture.

In this respect the area of elastography offers great promise. Elastography is concerned with the measurement of the stiffness of tissues in the individual patient, using MRI [14], or ultrasound [15]. The underlying physical principle in elastography is that the local displacement field resulting from shear wave propagation is directly related to the local shear modulus of the tissues. In both MRI elastography (called 'magnetic resonance elastography' or MRE) and ultrasound elastography, shear waves are induced in the tissues and the imaging system is used to track the shear waves and measure the shear modulus.

In MRE an external driver induces shear waves into the tissue whilst a synchronised motion-encoding gradient (MEG) is utilised to encode the resulting displacements in the MR phase image [16, 17]. Phase images taken at pre-determined time points typically over the course of one whole wave cycle at the frequency of the induced wave are used to create maps of displacement or wave images. These wave images are then processed using an inversion algorithm which estimates the shear wave wavelength from the MRI displacement field. From this the local elastic modulus is calculated. To date MRE has been applied to a wide variety of organs including the liver, brain, aorta, kidneys, lungs, heart and muscle [18, 19, 20, 21, 22, 23, 24, 25].

Acquisition of material properties through inversion is limited as a result of the assumptions that are used for their derivation [26, 27, 28]. Whilst these assumptions vary depending upon which inversion algorithm has been employed, in the most commonly

used algorithms typical assumptions are that the induced waves propagate through a linear viscoelastic medium which is infinite, isotropic and homogenous [28]. The results are also affected by constructive and destructive interference caused by wave scattering and reflections [29].

Computational modelling may be used for the testing and development of MRE post-processing software [30, 31, 32, 33] and in some instances as part of the inversion algorithm itself [34]. Essentially the entire measurement process from patient to elastogram is simulated. This includes the relevant patient anatomy (using idealised geometries generated in CAD), induction of shear waves and formation of the subsequent MRI displacement field (using FEA), and estimation of elastic properties (using wave inversion). This allows *in silico* experiments to be performed to assess the parameters in the MRE methodology and to obtain quantitative data on issues of clinical interest such as minimum lesion size which may be observed on the elastogram.

Whist the majority of the literature making use of FEA in the MRE field have utilised simplistic geometries, often with uniform material properties throughout, several papers have investigated specific anatomical structures. Notably Thomas-Seale et al. (2011) [33] demonstrated that high-frequency MRE had potential in differentiating the size of a lipid pool within an atherosclerotic plaque utilising a steady-state FEA technique. More recently Dao et al. (2014) [35] presented work which aimed to develop FEA of MRE in thigh skeletal muscle using 3-D geometries reconstructed from MRI datasets.

The aim of this paper is to use FEA to perform a preliminary investigation into the ability of MRE to achieve accurate and reproducible measurements of the elastic properties of the thrombus in different sized idealised AAA geometries. To achieve this 3-D axisymmetric idealised AAA geometries were created and the size and shear modulus of these AAAs was varied along with the frequency of the induced shear vibrations.

2. Methods

FEA has been performed with *Abaqus/explicit (Dassault Systeme Simulia Corp., Providence, Rhode Island, USA)* based on the methodologies previously described in Hollis et al. (2016 and 2016a) [36, 37] (figure 1).

2.1. Geometries

Computer aided design (CAD) in *Autodesk Autocad Student Version 2015 (Autodesk, Inc., San Rafael, California, USA)* was used to create 3-D idealised axisymmetric AAA geometries of diameter 50, 60 and 70 mm. All AAAs were designed such that the length from the proximal neck to distal neck was 90 mm based on measurements from Hans et al. (2005) [38] and consisted of a cylindrical lumen of radius 9 mm, a thrombus and a 2 mm thick vessel wall. Once completed the AAAs were encased in a cuboid box, whose size was varied depending upon the size of the AAA with the smallest distance from

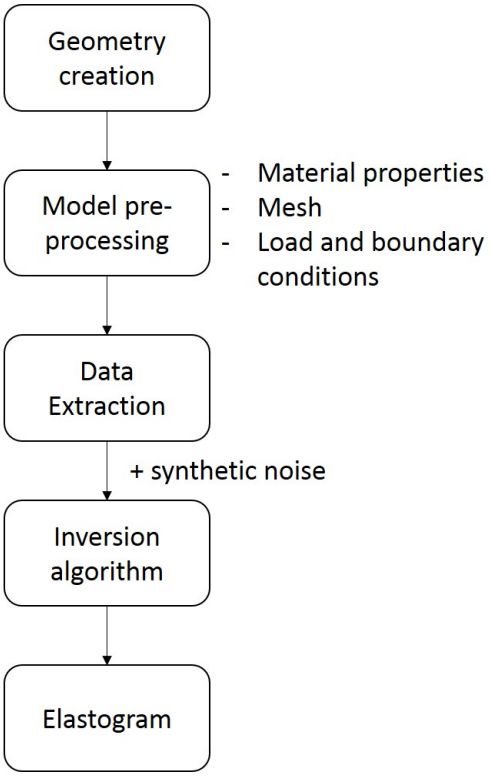

Figure 1. Workflow for FEA of MRE. Following extraction from the modelling software package and addition of noise, the synthetic data is fed directly into post-processing software used for analysing *in vivo* MRE datasets.

AAA to the edge of the box at the anterior being 20 mm and 10 mm on all other sides. To reduce the size of the model and the simulation time 15 mm were cut from the top and bottom of the model to reduce the length to 60 mm. Finally the different sections of the model were tied together using constraints (figure 2).

2.2. Modelling Setup

2.2.1. Load A harmonic load was applied to a set of nodes on the anterior surface of the model in the z-direction. The size of this region was consistent throughout all of the models. Frequencies of 50, 100 and 120 Hz were applied to each model.

2.2.2. Boundary Conditions Boundary conditions were applied to all surfaces apart from that upon which the load was applied. Displacements were fixed in the y-direction but left unconstrained in x and z.

2.2.3. Mesh Models were meshed using quadratic tetrahedral elements consisting of 10 nodes (C3D10M). The element length was defined as 2 mm along each edge within the model meaning that the models were constructed from 234,167, 237,312 and 246,532 elements for the respective 50, 60 and 70 mm size AAAs. Convergence studies were performed based on the criteria outlined in Hollis et al. (2016) [37] with element edge

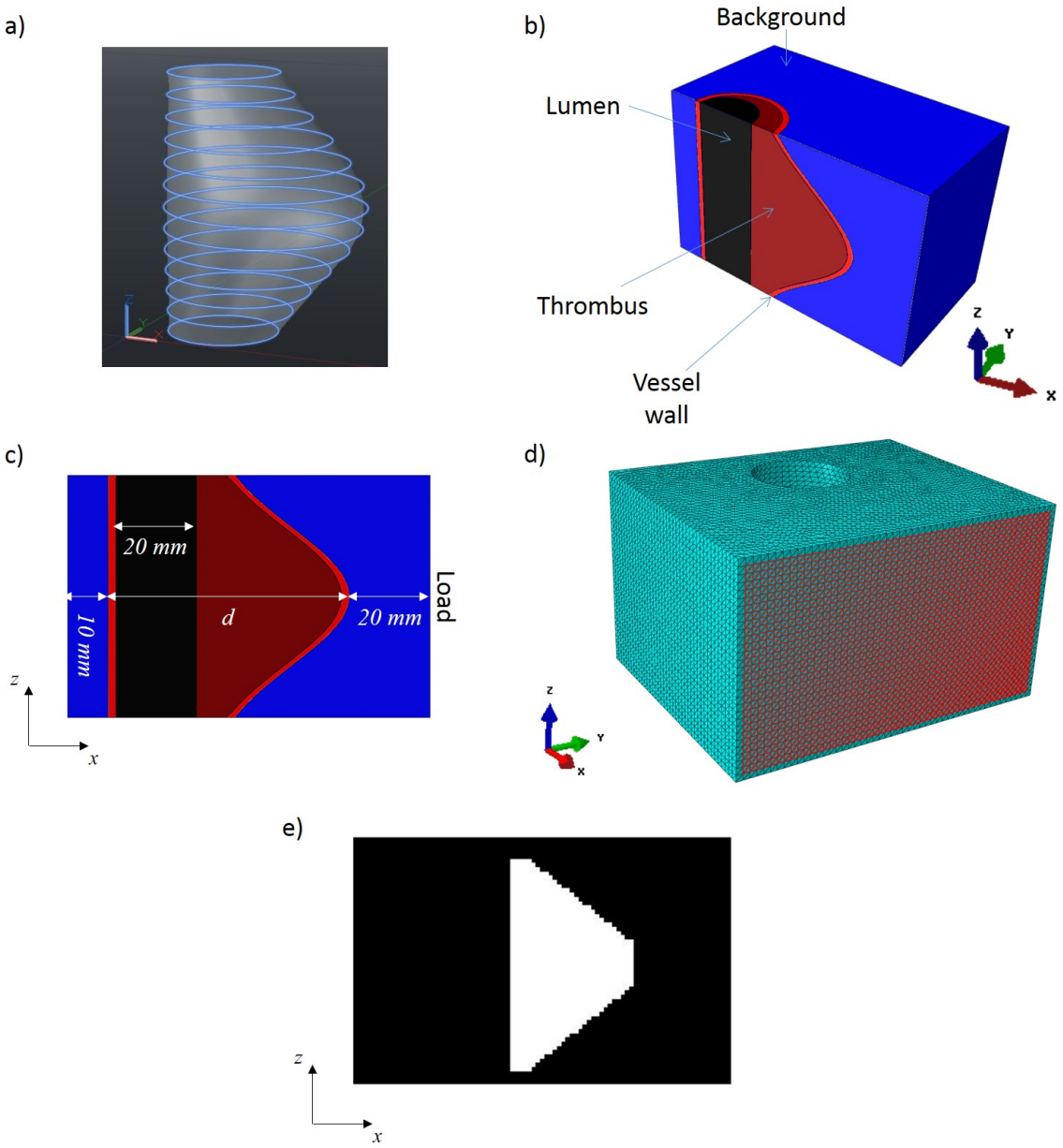

Figure 2. a) Idealised AAA geometries were created in *Autocad*. b) 3-D representation of the idealised 60 mm AAA showing the different components of the model. c) 2-D representation of the idealised 60 mm AAA showing the dimensions of the model. d represents the diameter of the AAA varied from 50-70 mm in this study. d) The load was applied in the z-direction to the anterior surface of the model via a set of nodes (displayed here in red) with a cross sectional area of 56×96 mm^2. e) The ROI for the 60 mm model to calculate the storage modulus of the thrombus.

lengths of 1.25, 2, 3 and 5 mm to ensure that an adequate mesh density for accurate simulation was selected.

2.3. Material Properties

All sections in the model were prescribed a density of 1047 kg·m^{-3} and adhered to the Kelvin-Voigt model of viscoelasticity, where the complex shear modulus, G^*, is given by [39]:

$$G^* = G + i\omega\eta \tag{1}$$

Here G is the shear storage or storage modulus, ω is the angular frequency and η is the shear viscosity, assumed as 1 Pa·s throughout all materials in the model.

2.3.1. Vessel Wall The storage modulus of the vessel wall was varied from 0.1 - 1.1 MPa based on values measured using mechanical testing [40, 41, 42, 43]. When investigating how variations in the shear storage modulus of the thrombus affect measurements, the shear storage modulus of the vessel wall was maintained at 0.7 MPa.

2.3.2. Thrombus Based on values measured by van Dam et al. (2006 and 2008) [44, 45] using shear loading, and Gasser et al. (2008) [46] using quasi-static loading, the shear modulus of the thrombus was varied from 1-21 kPa. When investigating how variations in the shear storage modulus of the vessel wall affect measurements, the shear storage modulus of the thrombus was maintained at 9 kPa.

2.3.3. Surrounding Tissue For the purposes of this study it was assumed that the surrounding tissue was fatty soft tissue. Whilst, to this authors knowledge, no such tissue has been examined in the abdomen, there have been studies of fatty soft tissue in heel pads [47] and breasts [48] and on both occasions has been characterised using MRE as having a shear storage modulus of approximately 8 kPa. Based on these papers the shear storage modulus of the surrounding tissue was defined as 8 kPa.

2.3.4. Lumen To model the lumen accurately would require an FSI simulation which would be highly computationally demanding and also incompatible with the viscoelastic properties employed in these models. The lumen was therefore modelled as a linear viscoelastic medium, like the rest of the model, with a low shear storage modulus of 0.1 kPa. An approach similar to this has previously been used to model lipid pools in atherosclerotic plaques [49, 50].

2.4. Post-Processing

2.4.1. Data Formatting Nodal displacements and coordinates were extracted from the *.odb* file created during simulation by *Abaqus* and imported into *Matlab R2013a (Mathworks, Natick, Massachusetts, USA)*. Displacements were then interpolated to evenly spaced points in 5 central *xy*-planes through the model, essentially replicating 5 slices from an MRE scan. The spacing between the *xy*-planes was matched to the spacing between points within that plane such that each point was effectively seen as

	1.5 mm^3	2 mm^3	2.5 mm^3	3 mm^3
50 mm	53×40×5	40×30×5	32×24×5	26×20×5
60 mm	60×40×5	45×30×5	36×24×5	30×20×5
70 mm	66×40×5	50×30×5	40×24×5	33×20×5

Table 1. Summary of the 3-D matrix sizes for each sized AAA for each voxel size.

representative of an isotropic voxel from an MRE scan. To investigate the effects of MRE voxel size, the spacing between interpolation points was varied, with spacings of 1.5, 2, 2.5 and 3 mm investigated. Table 1 summarises the imported matrix sizes for the various models and voxel sizes.

2.4.2. Inversion Inversion was performed using the 3-D direct inversion algorithm [51]:

$$G^* = -\rho\omega^2 \cdot \frac{\mathbf{a}}{\nabla^2 \mathbf{a}} \tag{2}$$

where ρ is the density, ω is the angular frequency and $\mathbf{a} = \nabla \times \mathbf{u}$, the curl of the displacement, incorporated to remove effects caused by the compressional wave [52]. As such, the shear storage modulus is calculated by taking the real part of G^*.

2.4.3. Noise and Filtering Noise was simulated and added to the complex waves using the technique outlined in Miller et al. (2015) [53] at levels ranging from 1-20%. A 3-D Butterworth bandpass filter was applied to these noisy complex wave images prior to inversion [54]. To determine the optimal filter widths that should be used, the filters ability to preserve measurements was tested on the noise free complex wave images across the range of prescribed shear moduli, with the following factor (termed the filter preservation scores from here on) used as guidance in this regard:

$$f = \sum_{n=1}^{N} \frac{\left(G_n^f - G_n^u\right)}{G_n^u} \tag{3}$$

Here G^u was the measured shear storage modulus when no filter was applied, G^f the measured shear modulus following application of the filter and N the number of different prescribed shear storage modulus values for the thrombus. The more effective the filter was in preserving the initial shear storage modulus measurement in noise free conditions, the lower this factor was. The lower cutoff with respect to the wavelength of the wave was varied from 1-3 voxel lengths and of order 5, whilst the higher cutoff was varied from 10-30 and of order 2.

2.4.4. Data Analysis Regions of interest (ROIs) were selected in the thrombus regions of the elastogram and the mean shear storage modulus within this region calculated. The ROIs were created manually such that areas within 2 pixels of the vessel wall and the edge of the model were excluded. The coefficient of variation, expressed here as a

percentage, was used to assess the variability of measurements across the different AAA sizes for each prescribed thrombus shear storage moduli:

$$c_v = 100 \cdot \frac{\sigma}{\mu} \tag{4}$$

where μ and σ represent the mean and standard deviation of the measurements respectively.

3. Results

3.1. Vessel Wall Shear Storage Modulus

Measurements of the shear storage modulus of the thrombus were relatively consistent for wave induced at 100 and 120 Hz. At 50 Hz however, increasing the prescribed shear storage modulus of the vessel wall resulted in a slight decrease in the measured value (figure 5*a*).

3.2. AAA Size and Stiffness

Increasing the prescribed shear storage modulus for the thrombus resulted in an increase in the measured value for all frequencies (figure 3). Accuracy depended upon both the prescribed shear storage modulus and frequency: greatest accuracy was typically achieved with 120 Hz vibrations, whilst poorest accuracy was achieved with the 50 Hz vibrations. The exception to this was for a prescribed shear storage modulus of 1 kPa, where vibrations induced at both 100 and 120 Hz resulted in large overestimations (mean errors across the three AAA sizes were 98% and 154% respectively). Variability of measurements was typically lowest at 120 Hz: the mean coefficients of variability across all prescribed shear storage moduli were 18, 11 and 9% for the 50, 100 and 120 Hz waves respectively (figure 5*a*-*c*).

3.3. Voxel Size

Increasing the voxel size typically increased the measurements made for all frequencies and prescribed shear moduli. Typically the coefficient of variation was greater for a voxel size of 3 mm^3 than the other sizes tested (figure 5*d*).

3.4. Noise and Filtering

For the 50 Hz waves, several filter limits achieved similar filter preservation scores in the range of 0.5-0.6. A lower cutoff of 1 and an upper cutoff of 15 were selected for application to the noisy data since, although these limits did not achieve the lowest score (0.56), they represented the narrowest filter in the 0.5-0.6 range. For both 100 and 120 Hz a lower cutoff of 3 and an upper cutoff of 20 comfortably achieved the lowest filter preservation scores (0.28 and 0.25 respectively) and were therefore used as the filter limits at these frequencies.

Addition of noise to the complex waves resulted in a decrease in the measured shear storage modulus values before application of the filter; the extent of this decrease was greater with increasing noise levels and prescribed shear storage moduli. At low noise levels of 1 or 2%, measurements following application of the bandpass filter were similar to measurements made on the unfiltered noise free data for all prescribed shear storage moduli. At higher noise levels than this, however, measurements from the filtered complex waves reduced in comparison to those from the unfiltered noise free data, although the size of this reduction was lower than when the noisy data was inverted without having been bandpass filtered first (figure 5*f*).

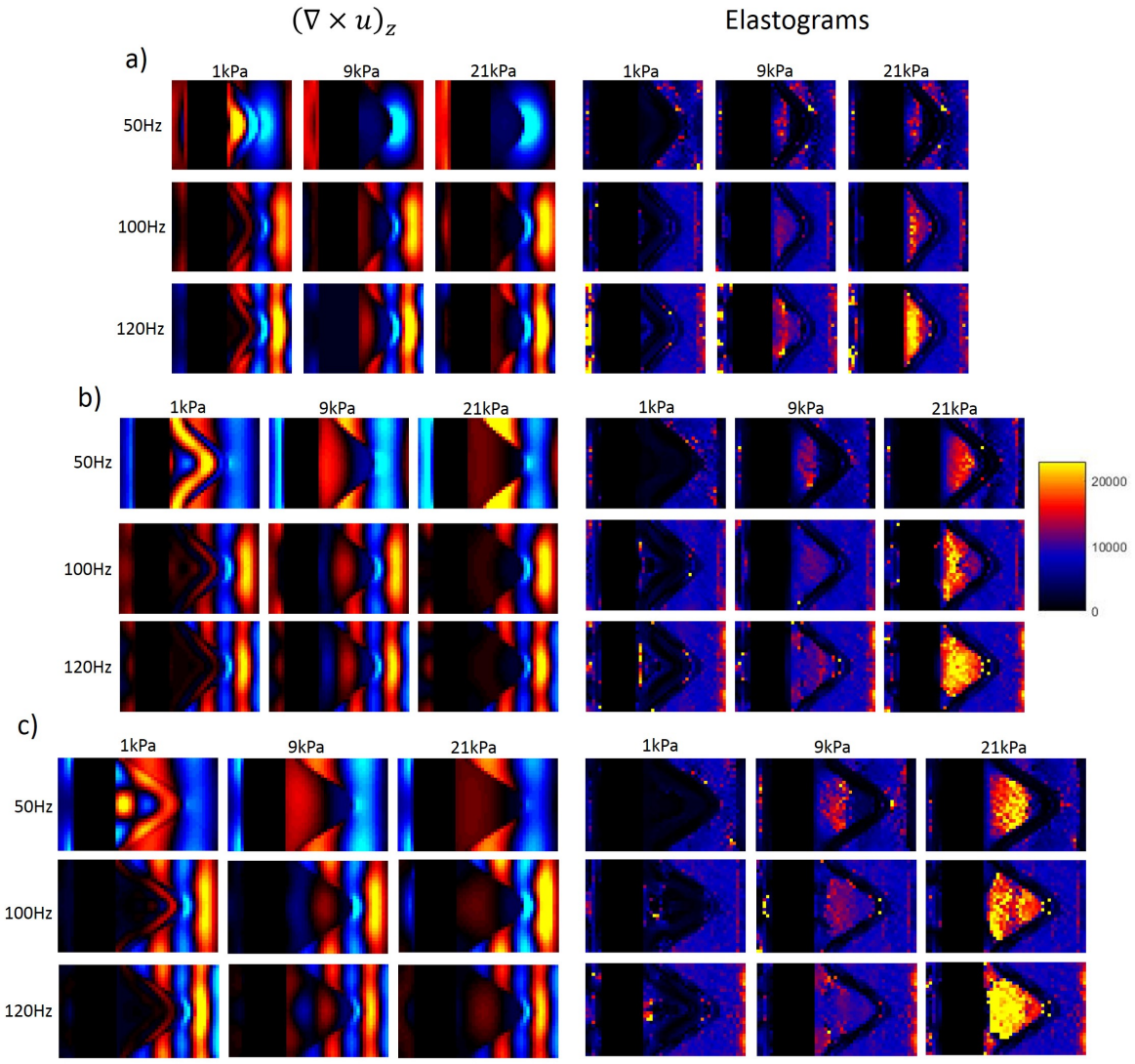

Figure 3. Curl of the complex displacements and the corresponding elastograms for the a) 50mm, b) 60mm and c) 70mm AAAs.

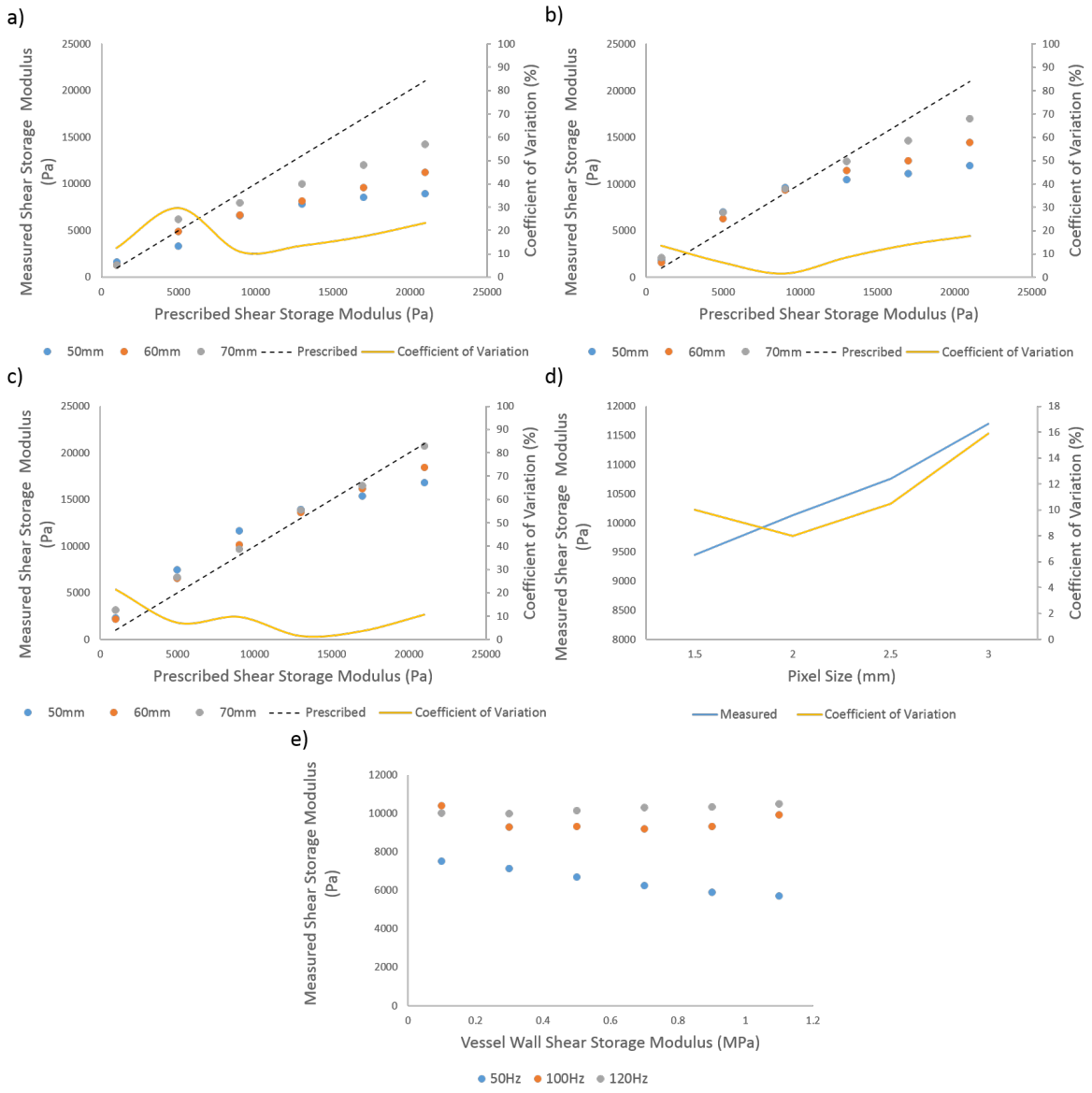

Figure 4. a) - c) Measured shear storage modulus measurements and the coefficient of variation between the three measurements against the prescribed thrombus shear storage modulus at 50, 100 and 120 Hz respectively. In all cases increasing the prescribed value resulted in an increase in measured value, however, measurements were not reproducible across the three AAA sizes for any frequency. The mean coefficient of variation for all prescribed shear storage moduli was lowest for 120 Hz. d) Measured shear storage modulus for a prescribed shear storage modulus of 9 kPa at 120 Hz and mean coefficient of variation across all prescribed values at 120 Hz against pixel size. Increasing the pixel size increased the measurement made. The coefficient of variability increased for a pixel size of 3 mm. e) Measured value for the thrombus against the prescribed shear storage modulus of the vessel wall. For waves induced at 50 Hz, despite the prescribed value of the thrombus being fixed, the measured value decreased as the prescribed value for the vessel wall was increased.

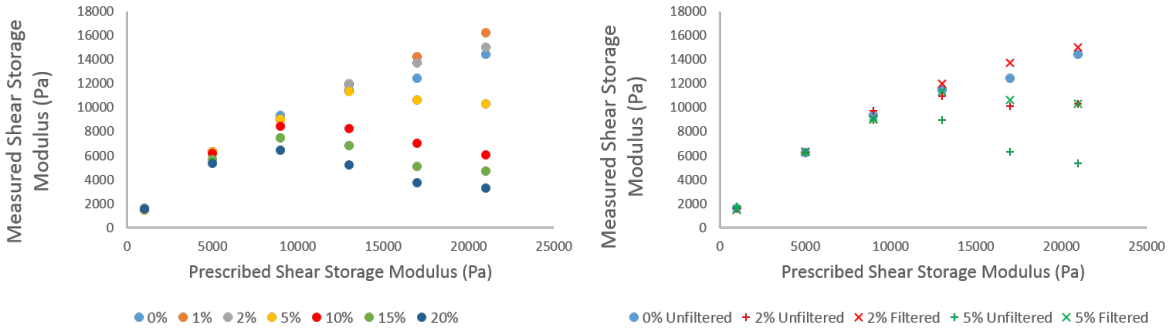

Figure 5. Graphs from the 60 mm AAA vibrated at 100 Hz. a) Measurements made from the unfiltered elastograms following the application of noise. Increasing noise levels reduced the values of the measurement made. b) Measurements made before and after the application of the Butterworth bandpass filter for noise levels of 2 and 5%. The filter was able to recover the measured values at low noise levels when compared to the noise free data.

4. Discussion

PSM of AAAs is limited by the lack of patient specific material properties, with several studies demonstrating the influence of the elastic properties of the thrombus upon stress in the AAA wall [55, 56]. Whilst MRE has the potential to provide inputs for this data, the geometrical dependence of the technique [37] raised concerns that such measurements would be inconsistent across the range of AAA shapes and sizes in the patient population. Utilising FEA in idealised geometries, this study demonstrated variations in measurements in three different sized AAAs with the same prescribed shear modulus. In stiffer materials, the wavelength of a lower frequency wave is long in comparison to the ROI [27, 57], thus accuracy of measurement is comprised. In contrast, in the Kelvin-Voigt model of viscoelasticty the shear loss modulus increases with frequency, whilst the shear storage modulus remains the same. Additionally, the loss and storage moduli are independent of one another, meaning that the loss component becomes increasingly dominant for lower storage modulus values. As such, wave damping is increased in low stiffness materials at high frequencies, resulting in increased artefacts following inversion and a reduction in accuracy of measurements (figure 3). Despite accuracy being compromised at 1 kPa for the 120 Hz vibrations as a result of this process, this frequency achieved the greatest accuracy in measurements above 1 kPa and greatest reproducibility in measurements between the different AAA sizes. It is recognised that inaccuracy of high frequency vibrations in low storage moduli materials is dependent on the viscoelastic model used in this study and not directly applicable to human tissue, which is typically not well represented by the Kelvin-Voigt model [58, 59]. The induction of waves of such a high frequency into an AAA, meanwhile, presents a significant technical challenge *in vivo*.

A further complication of *in vivo* MRE datasets is the inherent noise which effects the quality of elastograms and measurements. The post-processing pipeline in MRE

therefore typically involves application of a Butterworth bandpass filter, the aim of which is to remove noise whilst preserving information relating to the shear wave [54]. *In silico* experimentation outputs noise-free data providing an opportunity to test a variety of limits and help identify the narrowest width that best preserves the wanted information, thereby limiting effects that may occur through over-filtering. In this study noise was shown to have a dramatic influence on the measured values and the quality of the resulting elastogram. Application of the bandpass filter was visibly able improve the quality of the elastograms from noisy data (figure 6), but was only able to recover the measured values to approximate those in noise-free conditions at low levels. This emphasises the importance of obtaining displacement images with as little noise as possible in the MR scan; again a significant technical challenge given the large amount of natural body motion in this region of the anatomy. To this end increased signal-to-noise ratio (SNR) in MRI is associated with voxel size. Whilst measurements increased here with voxel size, in likelihood due to discretisation errors [28], the coefficient of variation remained similar for voxels up to a size of 2.5 mm^3. This implies that SNR could potentially be increased by utilising a larger voxel size, without compromising on the reproducibility of measurements between different sized AAAs.

A recognised limitation of this study is in the material properties applied, with literature values varying greatly depending on the technique used to make measurements, and limited information as to the viscoelastic properties of these materials. To date no MRE studies have investigated AAAs meaning that material properties were prescribed based upon measurements taken by other techniques. Whilst measurements have been made of the vessel wall material properties through dynamic loading [60, 61, 62], these have been of healthy porcine and canine aorta, with diseased and human aortic stiffnesses known to differ dramatically [40, 63]. As a result, the elastic properties of the vessel wall were based on measurements made using static loading alone. It is acknowledged that these are likely to differ from measurements made using dynamic loading in the frequency range of interest in this study [61].

Since this study aimed to focus primarily on the influence of geometry upon measurements, the Kelvin-Voigt model of viscoelasticity was employed. The advantage of this model is that the elastic and viscous properties are independent of one another thus allowing direct comparison of measurements of elastic properties from different frequencies. In this regard, it is worth noting that in studies by van Dam et al. (2006 and 2008) [44, 45] using shear loading to investigate viscoelastic properties of thrombus, inter-patient variability in the elastic properties was greater than the variation in measurements across the wide range of frequencies used. The viscous properties applied in this study were in the range of those attained for the thrombus by van Dam [44, 45]. It is however, a recognised limitation that whilst MRE is capable of achieving measurements relating to both the elastic and viscous components of the shear modulus, the present study has focused upon the elastic properties alone. Further *ex vivo* studies of the material properties, both elastic and viscous, of the thrombus, vessel wall and surrounding tissue with MRE would prove useful in determining the range of values

and complexity of the material models employed in future investigations. This would allow *in silico* experimentation to determine the extent to which the viscous properties influence the stress acting on the AAA wall and the accuracy with which MRE is able attain measurements of these properties. Additionally more complex models using CFD incorporated into a fluid-structure interaction (FSI) simulation to better replicate the blood would allow for investigation into how the pulse wave affects stiffness of the AAA.

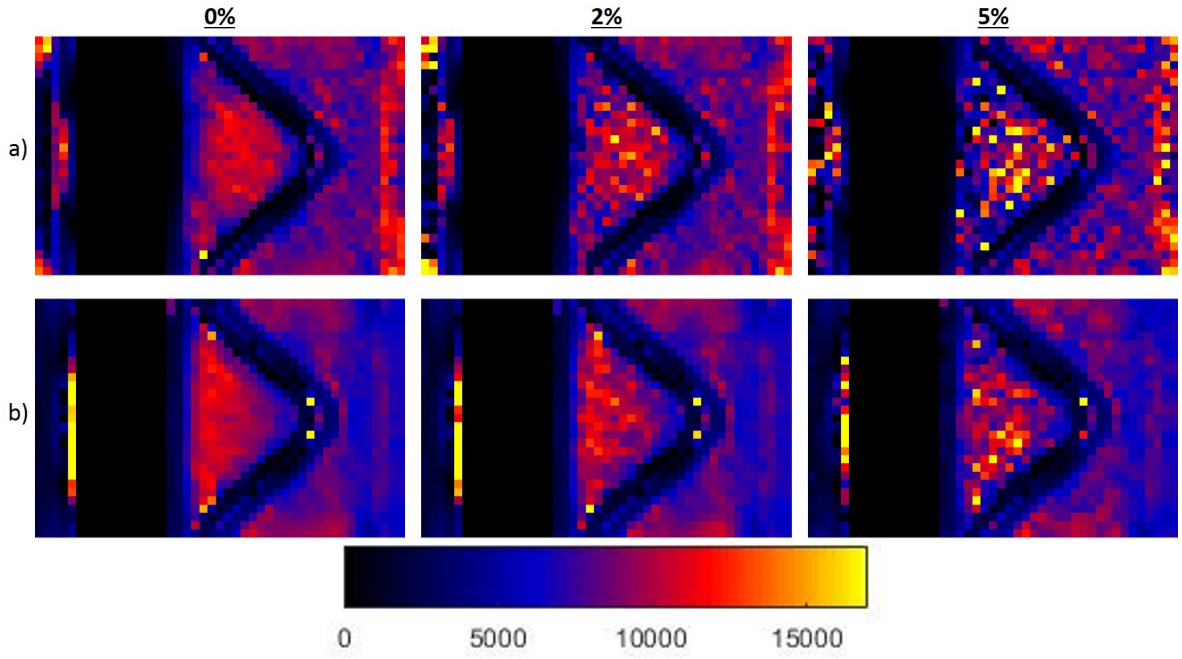

Figure 6. a) Unfiltered and b) filtered elastograms for the 60 mm diameter 9 kPa AAAs vibrated at 100 Hz. The filter has relatively little effect upon the noise-free elastogram, but is noticeably able to reduce improve the quality of the elastograms at noise levels of 2 and 5%.

5. Conclusion

This study used idealised geometries to investigate the reproducibility of MRE measurements of AAA thrombus. Accuracy in measurements from AAAs with high prescribed shear moduli increased with frequency, whilst the opposite was true for AAAs prescribed with low shear moduli. Variability in measurements across the three AAA sizes was lowest at 120 Hz with a mean coefficient of variation across all prescribed shear moduli of 9% in contrast to 18% and 11% for 50 and 100 Hz respectively. Higher frequencies were less susceptible to the changes in the shear modulus of the vessel wall. Noise affected both the quality of the elastograms and the measurements made. Application of a Butterworth bandpass filter with limits identified from the noise-free data fully recovered material property measurements at low noise levels of 1 or 2%, but was not able to do so at noise levels of 5% and over. Though preliminary, this study suggests that, despite poor accuracy of measurements in low stiffness AAAs, with

regards to acquiring accurate and reproducible measurements across the full range of prescribed shear moduli tested here, an applied frequency of 120 Hz presents as the optimum in these geometries.

6. Appendix

Code relating to the work carried out in this paper has been uploaded to:

https://github.com/lyamhollis/abaqus_to_matlab

and is freely available for use. This includes the *Python* codes for exporting data from the *Abaqus .odb* files and the *Matlab* functions used to import this data, perform inversion, and bandpass filter the data.

7. Acknowledgements

This work was supported by funding from the British Heart Foundation.

References

[1] ML Neal and R Kerckhoffs. Current progress in patient-specific modeling. *Briefings in bioinformatics*, 11(1):111–26, 2010.

[2] CA Taylor and CA Figueroa. Patient-specific modeling of cardiovascular mechanics. *Annual review of biomedical engineering*, 11:109–34, 2009.

[3] GY Suh, AS Les, AS Tenforde, SC Shadden, RL Spilker, JJ Yeung, CP Cheng, RJ Herfkens, RL Dalman, and CA Taylor. Hemodynamic changes quantified in abdominal aortic aneurysms with increasing exercise intensity using mr exercise imaging and image-based computational fluid dynamics. *Annals of biomedical engineering*, 39(8):2186–202, 2011.

[4] PR Hoskins and D Hardman. Three-dimensional imaging and computational modelling for estimation of wall stresses in arteries. *The British journal of radiology*, 82 Spec No:S3–17, 2009.

[5] TC Gasser, G Martufi, M Auer, M Folkesson, and J Swedenborg. Micromechanical characterization of intra-luminal thrombus tissue from abdominal aortic aneurysms. *Ann Biomed Eng*, 38(2):371–9, 2010.

[6] C Reeps, M Gee, A Maier, M Gurdan, HH Eckstein, and WA Wall. The impact of model assumptions on results of computational mechanics in abdominal aortic aneurysm. *Journal of vascular surgery*, 51(3):679–88, 2010.

[7] ML Raghavan, DA Vorp, MP Federle, MS Makaroun, and MW Webster. Wall stress distribution on three-dimensionally reconstructed models of human abdominal aortic aneurysm. *J Vasc Surg*, 31(4):760–9, 2000.

[8] DHJ Wang, MS Makaroun, MW Webster, and DA Vorp. Effect of intraluminal thrombus on wall stress in patient-specific models of abdominal aortic aneurysm. *Journal of Vascular Surgery*, 36(3):598–604, sep 2002.

[9] A Maier, MW Gee, C Reeps, HH Eckstein, and WA Wall. Impact of calcifications on patient-specific wall stress analysis of abdominal aortic aneurysms. *Biomech Model Mechan*, 9(5):511–21, 2010.

[10] BJ Doyle, A Callanan, PE Burke, PA Grace, MT Walsh, DA Vorp, and TM McGloughlin. Vessel asymmetry as an additional diagnostic tool in the assessment of abdominal aortic aneurysms. *Journal of vascular surgery*, 49(2):443–54, 2009.

[11] L Speelman, A Bohra, EH Bosboom, GWH Schurink, FN van de Vosse, MS Makaorun, and DA Vorp. Effects of wall calcifications in patient-specific wall stress analyses of abdominal aortic aneurysms. *J Biomech Eng*, 129(1):105–9, feb 2007.

[12] ML Raghavan, JA Kratzberg, and J Golzarian. Introduction to biomechanics related to endovascular repair of abdominal aortic aneurysm. *Techniques in vascular and interventional radiology*, 8(1):50–5, 2005.

[13] AK Venkatasubramaniam, MJ Fagan, T Mehta, KJ Mylankal, B Ray, G Kuhan, IC Chetter, and PT McCollum. A comparative study of aortic wall stress using finite element analysis for ruptured and non-ruptured abdominal aortic aneurysms. *Eur J Vasc Endovasc Surg*, 28(2):168–76, 2004.

[14] R Muthupillai, DJ Lomas, PJ Rossman, JF Greenleaf, A Manduca, and RL Ehman. Magnetic resonance elastography by direct visualization of propagating acoustic strain waves. *Science*, 269(5232):1854–7, 1995.

[15] J Ophir, I Cespedes, H Ponnekanti, Y Yazdi, and X Li. Elastography: A quantitative method for imaging the elasticity of biological tissues. *Ultrasonic Imaging*, 13(2):111–134, 1991.

[16] A Manduca, R Muthupillai, PJ Rossman, JF Greenleaf, and RL Ehman. Local wavelength estimation for magnetic resonance elastography. In *Proceedings of 3rd IEEE International Conference on Image Processing*, volume 3, pages 527–530. IEEE, 1996.

[17] TE Oliphant, A Manduca, RL Ehman, and JF Greenleaf. Complex-valued stiffness reconstruction for magnetic resonance elastography by algebraic inversion of the differential equation. *Magnet Reson Med*, 45(2):299–310, 2001.

[18] O Rouvière, R Souchon, G Pagnoux, JM Ménager, and JY Chapelon. MR Elastography of the kidneys: feasibility and reproducibility in young healthy adults. *J Magn Reson Im*, 34(4):880–886, 2012.

[19] M Yin, JA Talwalkar, and KJ Glaser. A preliminary assessment of hepatic fibrosis with magnetic resonance elastography. *Clinical Gastroenterology and Hepatology*, 5(10):1207–1213, 2007.

[20] A Kolipaka, D Woodrum, PA Araoz, and RL Ehman. MR elastography of the in vivo abdominal aorta: a feasibility study for comparing aortic stiffness between hypertensives and normotensives. *J Magn Reson Im*, 35(3):582–6, 2012.

[21] A Kolipaka, KP McGee, A Manduca, AJ Romano, KJ Glaser, PA Araoz, and RL Ehman. Magnetic resonance elastography: Inversions in bounded media. *Magnet Reson Med*, 62(6):1533–42, 2009.

[22] YK Mariappan, KJ Glaser, RD Hubmayr, A Manduca, RL Ehman, and KP McGee. MR elastography of human lung parenchyma: technical development, theoretical modeling and in vivo validation. *J Magn Reson Im*, 33(6):1351–61, jun 2011.

[23] Thomas Elgeti, Jens Rump, Uwe Hamhaber, Sebastian Papazoglou, Bernd Hamm, Jürgen Braun, and Ingolf Sack. Cardiac magnetic resonance elastography: initial results. *Investigative Radiology*, 43(11):762–772, 2008.

[24] A Kolipaka, PA Araoz, KP McGee, A Manduca, and RL Ehman. Magnetic resonance elastography as a method for the assessment of effective myocardial stiffness throughout the cardiac cycle. *Magnet Reson Med*, 64(3):862–70, sep 2010.

[25] E Barnhill, P Kennedy, S Hammer, EJR van Beek, C Brown, and NR Roberts. Statistical mapping of the effect of knee extension on thigh muscle viscoelastic properties using magnetic resonance elastography. *Physiol Meas*, 34(12):1675–98, 2013.

[26] M Honarvar, R Sahebjavaher, R Sinkus, R Rohling, and S Salcudean. Curl-based Finite Element Reconstruction of the Shear Modulus Without Assuming Local Homogeneity: Time Harmonic Case. *IEEE transactions on medical imaging*, 2013.

[27] R Sinkus, JL Daire, BE Van Beers, and V Vilgrain. Elasticity reconstruction: Beyond the assumption of local homogeneity. *Comptes Rendus Mécanique*, 338(7-8):474–479, 2010.

[28] S Papazoglou, U Hamhaber, J Braun, and I Sack. Algebraic Helmholtz inversion in planar magnetic resonance elastography. *Phys Med Biol*, 53(12):3147–58, 2008.

[29] S Papazoglou. *Elucidation of Isotropic and Anisotropic Shear Elasticity of in vivo Soft Tissue using Planar Magnetic Resonance Elastography*. PhD thesis, 2009.

[30] Q Chen, SI Ringleb, A Manduca, RL Ehman, and KN An. A finite element model for analyzing shear wave propagation observed in magnetic resonance elastography. *J Biomech*, 38(11):2198–203, 2005.

[31] GE Leclerc, F Charleux, MC Ho Ba Tho, and SF Bensamoun. Identification process based on shear wave propagation within a phantom using finite element modelling and magnetic resonance elastography. *Comput Method Biomech*, (September 2014):37–41, 2013.

[32] KP McGee, D Lake, Y Mariappan, RD Hubmayr, A Manduca, K Ansell, and RL Ehman. Calculation of shear stiffness in noise dominated magnetic resonance elastography data based on principal frequency estimation. *Physics in medicine and biology*, 56(14):4291–309, 2011.

[33] LEJ Thomas-Seale, D Klatt, P Pankaj, N Roberts, I Sack, and P Hoskins. A simulation of the magnetic resonance elastography steady state wave response through idealised atherosclerotic plaques. *IAENG Int J Comput Sci*, 38(4):2636–39, 2011.

[34] EE Van Houten, KD Paulsen, MI Miga, FE Kennedy, and JB Weaver. An overlapping subzone technique for MR-based elastic property reconstruction. *Magnet Reson Med*, 42(4):779–86, oct 1999.

[35] TT Dao, P Pouletaut, F Charleux, MHB Tho, and S Bensamoun. Analysis of shear wave propagation derived from MR elastography in 3D thigh skeletal muscle using subject specific finite element model. In *Conference Proceedings of IEEE Eng Med Biol Soc*, pages 4026–9, 2014.

[36] L Hollis, LEJ Thomas-Seale, N Conlisk, N Roberts, P Pankaj, and PR Hoskins. Investigation of Modelling Parameters for Finite Element Analysis of MR Elastography. *Computational Biomechanics in Medicine: Imaging, Modeling and Computing*, 2016.

[37] L Hollis, E Barnhill, N Conlisk, LEJ Thomas-Seale, N Roberts, P Pankaj, and PR Hoskins. Finite Element Analysis to Compare the Accuracy of the Direct and MDEV Inversion Algorithms in MR Elastography. *IAENG Int J Comput Sci*, 2016.

[38] SS Hans, O Jareunpoon, M Balasubramaniam, and GB Zelenock. Size and location of thrombus in intact and ruptured abdominal aortic aneurysms. *J Vasc Surg*, 41(4):584–8, 2005.

[39] HA Barnes, JF Hutton, and K Walters. *An introduction to rheology*. Elsevier, vol. 3 edition, 1989.

[40] ÁP Tierney, A Callanan, and TM McGloughlin. In vivo feasibility case study for evaluating abdominal aortic aneurysm tissue properties and rupture potential using acoustic radiation force impulse imaging. *Journal of the Mechanical Behavior of Biomedical Materials*, 4(3):507–513, 2011.

[41] TJ Corbett, BJ Doyle, A Callanan, MT Walsh, and TM McGloughlin. Engineering silicone rubbers for in vitro studies: creating AAA models and ILT analogues with physiological properties. *J Biomed Eng*, 132(1):1–25, 2010.

[42] M L Raghavan, M W Webster, and D a Vorp. Ex vivo biomechanical behavior of abdominal aortic aneurysm: assessment using a new mathematical model. *Annals of biomedical engineering*, 24(5):573–82, 1996.

[43] T. Lanne, B. Sonesson, D. Bergqvist, H. Bengtsson, and D. Gustafsson. Diameter and compliance in the male human abdominal aorta: Influence of age and aortic aneurysm. *European Journal of Vascular Surgery*, 6(2):178–184, 1992.

[44] Evelyne a van Dam, Susanne D Dams, Gerrit W M Peters, Marcel C M Rutten, Geert Willem H Schurink, Jaap Buth, and Frans N van de Vosse. Determination of linear viscoelastic behavior of abdominal aortic aneurysm thrombus. *Biorheology*, 43(6):695–707, jan 2006.

[45] EA van Dam, SD Dams, GWM Peters, MCM Rutten, GWH Schurink, J Buth, and FN van de Vosse. Non-linear viscoelastic behavior of abdominal aortic aneurysm thrombus. *Biomechanics and modeling in mechanobiology*, 7(2):127–37, 2008.

[46] TC Gasser, G Görgülü, M Folkesson, and J Swedenborg. Failure properties of intraluminal

thrombus in abdominal aortic aneurysm under static and pulsating mechanical loads. *Journal of vascular surgery*, 48(1):179–88, 2008.

[47] JB Weaver, M Doyley, Y Cheung, F Kennedy, EL Madsen, EEW Van Houten, and K Paulsen. Imaging the shear modulus of the heel fat pads. *Clin Biomech*, 20(3):312–9, mar 2005.

[48] EEW Van Houten, MM Doyley, FE Kennedy, JB Weaver, and KD Paulsen. Initial in vivo experience with steady-state subzone-based MR elastography of the human breast. *J Magn Reson Im*, 17(1):72–85, 2003.

[49] GA Holzapfel. Changes in the Mechanical Environment of Stenotic Arteries During Interaction With Stents: Computational Assessment of Parametric Stent Designs. *Journal of Biomechanical Engineering*, 127(1):166, 2005.

[50] DE Kiousis, SF Rubinigg, M Auer, and GA Holzapfel. A methodology to analyze changes in lipid core and calcification onto fibrous cap vulnerability: the human atherosclerotic carotid bifurcation as an illustratory example. *Journal of biomechanical engineering*, 131(12):121002, 2009.

[51] A Manduca, TE Oliphant, MA Dresner, JL Mahowald, SA Kruse, E Amromin, JP Felmlee, JF Greenleaf, and RL Ehman. Magnetic resonance elastography: non-invasive mapping of tissue elasticity. *Med Image Anal*, 5(4):237–54, 2001.

[52] R Sinkus, M Tanter, T Xydeas, S Catheline, J Bercoff, and M Fink. Viscoelastic shear properties of in vivo breast lesions measured by MR elastography. *Magnetic resonance imaging*, 23(2):159–65, 2005.

[53] RJH Miller, R Mazumder, B Cowan, M Nash, A Kolipaka, and A Young. Determining Anisotropic Myocardial Stiffness from Magnetic Resonance Elastography: A Simulation Study. In *Functional Imaging and Modelling of the Heart: 8th International Conference*, pages 346–354, 2015.

[54] A Manduca, DS Lake, SA Kruse, and RL Ehman. Spatio-temporal directional filtering for improved inversion of MR elastography images. *Med Image Anal*, 7(4):465–73, dec 2003.

[55] BJ Doyle, A Callanan, and TM McGloughlin. A comparison of modelling techniques for computing wall stress in abdominal aortic aneurysms. *Biomed Eng*, 6:38, jan 2007.

[56] WR Mower, WJ Quiñones, and SS Gambhir. Effect of intraluminal thrombus on abdominal aortic aneurysm wall stress. *J Vasc Surg*, 26(4):602–8, oct 1997.

[57] LEJ Thomas-Seale, L Hollis, D Klatt, I Sack, N Roberts, P Pankaj, and PR Hoskins. The simulation of magnetic resonance elastography through atherosclerosis. *Journal of Biomechanics*, apr 2016.

[58] Y Liu, TK Yasar, and TJ Royston. Ultra wideband (0.516kHz) MR elastography for robust shear viscoelasticity model identification. *Physics in Medicine and Biology*, 59(24):7717–7734, 2014.

[59] I Sack, J Rump, T Elgeti, A Samani, and J Braun. MR elastography of the human heart: noninvasive assessment of myocardial elasticity changes by shear wave amplitude variations. *Magnet Reson Med*, 61(3):668–77, mar 2009.

[60] DA Woodrum, AJ Romano, A Lerman, UH Pandya, D Brosh, PJ Rossman, LO Lerman, and RL Ehman. Vascular wall elasticity measurement by magnetic resonance imaging. *Magnet Reson Med*, 56(3):593–600, 2006.

[61] L Xu, J Chen, M Yin, KJ Glaser, Q Chen, DA Woodrum, and RL Ehman. Assessment of stiffness changes in the ex vivo porcine aortic wall using magnetic resonance elastography. *Magn Reson Imaging*, 30(1):122–7, jan 2012.

[62] DH Bergel. The dynamic elastic properties of the arterial wall. *The Journal of physiology*, pages 458–469, 1961.

[63] C Martin, T Pham, and W Sun. Significant differences in the material properties between aged human and porcine aortic tissues. *Eur J Cardio-Thorac*, 40(1):28–34, 2011.